Thermal Analysis of Alternative Diesel Fuels from Vegetable Oils[1]

Robert O. Dunn*

Oil Chemical Research, USDA, ARS, NCAUR, Peoria, Illinois 61604

ABSTRACT: The relatively poor cold-flow properties of monoalkyl esters of vegetable oils and animal fats (biodiesel) present a major obstacle to their development as alternative fuels and extenders for combustion in direct injection compression-ignition (diesel) engines. In this work, differential scanning calorimetry (DSC) heating and cooling curves of methyl soyate (SME), methyl tallowate (TME), SME/TME admixtures, and winterized SME were analyzed. Completion of melt, crystallization onset (Onset), and other temperatures corresponding to melting and freezing peaks were correlated to predict cloud point (CP), pour point (PP), cold filter plugging point (CFPP), and low-temperature flow test (LTFT) data. Effects of treating methyl esters with cold-flow improvers were examined. Low-temperature flow properties of biodiesel may be accurately inferred from subambient DSC analyses of high-melting or freezing (β-form) peaks. The temperature of maximal heat flow for freezing peaks gave the best accuracy for predicting CP, PP, and CFPP, while freezing point gave the best accuracy for predicting LTFT. Onset also gave good correlations with respect to predicting PP, CFPP, and LTFT. Cooling scan parameters were more reliable than heating scan parameters.

Paper no. J8917 in *JAOCS 76,* 109–115 (January 1999).

KEY WORDS: Cloud point, cold filter plugging point, crystallization onset, differential scanning calorimetry, freezing point, low-temperature flow test, melting point, methyl esters, pour point.

Monoalkyl esters of fatty acids derived from vegetable oil or animal fat (biodiesel) have properties that make them attractive as alternative fuels and extenders for combustion in compression ignition (diesel) engines. However, among the obstacles that must be resolved before biodiesel will be widely commercialized in North America is the problem of relatively poor low-temperature flow properties.

As ambient temperatures decrease toward the cloud point (CP), long-chain saturated molecules begin to form small crystal nuclei in diesel fuels. As temperatures decrease below CP, crystalline growth and agglomeration continue until the crystals become large enough to plug fuel lines. Crystals whose average particle size exceeds ~10 μm will restrict flow through filters. These conditions cause startup and operability problems that may lead to fuel starvation and engine failure. Operability problems generally develop in No. 2 diesel fuel when overnight temperatures approach the range of −10 to −15°C (1,2). Methyl soyate (SME) showed it may cause similar problems as temperatures approach 0°C (3).

Operability temperature limits for diesel fuels cannot be reliably predicted by CP or pour point (PP) measurements. Thus, the cold-filter plugging point (CFPP) and low-temperature flow test (LTFT) must be employed to predict operability limits (4,5). CFPP is the accepted test in Africa, the Asia-Pacific Rim, Europe, and South America. The more rigorous, less user-friendly LTFT is regarded as more reliable than CFPP for predicting operability limits in North America.

Earlier studies (3,6,7) showed that LTFT and CFPP of SME, SME-methyl tallowate (TME) admixtures, and SME/distillate blends were essentially linear functions of CP. Statistical analyses showed that an empirical 1:1 correlation exists between LTFT and CP (that is, LTFT = CP). Furthermore, treatment of blends of 10 + vol% SME with cold-flow improvers marketed for distillate fuels did not greatly affect CP, CFPP, or LTFT. These studies concluded that approaches for improving the low-temperature flow properties of biodiesel should first be evaluated for potential to reduce CP.

One technique for reducing CP is to decrease the total saturated ester concentration in biodiesel *via* winterization (7,8). Although winterization of neat SME gave poor yields (30–35 wt% relative to starting material), treatment with additives prior to winterization improved yields to >80%. Winterized products gave CP ≤−11°C, a value comparable to operability limits for No. 2 diesel fuel (9).

The success of other approaches, including developing new cold-blow improvers or surfactants to modify colligative properties, necessitates acquiring new fundamental knowledge relating to nucleation and crystal growth in biodiesel and biodiesel/distillate blends. Much study has been devoted to triglycerides and their fatty acids; however, relatively little emphasis was placed on corresponding fatty esters. This work examines the usefulness of subambient thermal analyses to meet the need for fundamental knowledge.

Heino (10) reported that CP of distillate fuels may be determined more accurately from differential scanning calorimetry

---

[1]Presented at the 88th American Oil Chemists' Society's Annual Meeting & Expo, Seattle, Washington, May 11–14, 1997.

*Address correspondence at Oil Chemical Research, USDA, ARS, NCAUR, 1815 N. University St., Peoria, IL 61604.
E-mail: dunnro@mail.ncaur.usda.gov

(DSC) than from American Society of Testing and Materials (ASTM) approved methods. That study showed that CP with repeatability <±0.7°C could be inferred from DSC cooling scans. Claudy *et al.* (11) reported that crystallization onset temperatures (Onset) from DSC cooling scans may be employed to determine CP, PP, and CFPP of diesel fuels containing no additives, and concluded that reproducibility of DSC analyses was more reliable than corresponding ASTM or European standard tests. Noel (12) and Redelius (13) obtained similar results for petroleum-based lubricants and other engine oils.

Earlier studies (6,9) reported that CP of SME may also be determined directly from DSC heating and cooling scans. These studies showed that Onset determined from cooling scans may be employed to predict CP within an estimated error of 1.8°C. These studies also showed that DSC analyses gave more reliable results than ASTM method D2500 (14). This work extends the applicability of DSC in measuring CP, PP, CFPP, and LTFT of nonwinterized SME, TME, SME/TME admixtures, and winterized SME formulations.

MATERIALS AND METHODS

Materials. SME from Interchem Environmental (Overland Park, KS) was provided by the National Biodiesel Board (Jefferson City, MO). Capillary gas chromatography (GC) analysis showed a fatty acid ester composition of 14.7 wt% hexadecanoate, 5.0% octadecanoate, 26.2% 9*Z*-octadecenoate, 44.4% 9*Z*,12*Z*-octadecadienoate, and 9.6% 9*Z*,12*Z*,15*Z*-octadecatrienoate. Physical properties were kinematic viscosity = 4.20 mm^2/s (40°C), specific gravity (SG) = 0.881 at 15.6°C relative to distilled water at 15.6°C, acid value = 0.16 mg KOH/g oil, peroxide value = 57.0 meq/kg oil, and calculated iodine value (IV) = 123 g I_2/100 g oil.

TME (Kemester 143) was from Witco (Memphis, TN). GC analysis showed 0.2 wt% tetradecanoate, 28.7% hexadecanoate, 2.6% hexadecenoate, 20.8% 9*Z*-octadecanoate, 43.0% 9*Z*-octadecenoate, 4.3% 9*Z*,12*Z*-octadecadienoate, and 0.4% 9*Z*,12*Z*,15*Z*-octadecatrienoate. Physical properties were kinematic viscosity = 6.07 mm^2/s, SG = 0.876, calculated IV = 48 g I_2/100 g oil, and flash point = 145°C (closed cup).

Winterflow, from Starreon Corp. (Englewood, CO), was a mixture of light and heavy petroleum naphtha, trimethyl benzene isomers, propylene glycol ether, xylene, hydroxyethylated aminoethylamide, cumene, and ethyl benzene. DFI-200, from Du Pont Chemical (Wilmington, DE), was a mixture of severely hydrotreated light naphthenic distillates and ethylene/vinyl acetate copolymers. Winterflow and DFI-200 were used as cold-flow improvers in nonwinterized formulations and as additives for winterization of SME.

Methods. Apparatus and methods for winterization of SME and SME-additive mixtures were described previously (9). Samples were step-by-step winterized at 2°C intervals starting at 0°C and terminating at −10°C.

Apparatus and methods for measuring CP, PP, and LTFT were in accordance with ASTM standard test methods (14–16) and those for measuring CFPP were in accordance with Institute of Petroleum method IP 309 (17). CP, PP, and CFPP results shown in Table 1 were mean values from three replicates; variances (σ^2) were 0.3333 for CP (of TME), 0.3333 for PP (of TME), and 0.2500–0.3333 for CFPP. LTFT results were for one replicate.

DSC analyses were conducted on a TA Instruments (New Castle, DE) model 2910 DSC with a model 2100 personal computer-based controller. The measurement cell was purged with low-pressure nitrogen gas and fitted with a liquid nitrogen-cooled heat exchanger for subambient scans. For each scan, ~10 mg of sample was hermetically sealed in an aluminum pan and tested against an identical empty pan. A ramp rate of 5°C/min was selected because it gave a good combination of resolution characteristics and timeliness. For heating scans, samples were rapidly cooled and held isothermally at −100°C for 10 min, then heated to 40°C. For cooling scans, samples were equilibrated at 40°C, then cooled to −100°C. Heat flow (W/g) vs. temperature (°C) curves obtained from heating DSC scans were analyzed to determine the following parameters: completion of melt onset temperature (COM), minimal heat-flow temperature of the high-melting peak (P1), and melting point (MP). The following parameters were obtained from cooling scans: Onset, maximal heat flow temperature of the high-freezing peak (P2), and freezing point (FP). Results listed in Table 2 were mean values (n = 2–6 replicates) with each measurement taken on a fresh oil sample to reduce bias due to irreversible transitions that may occur following cooling or heating. These mean values gave σ^2 values in the ranges of 0.0049–1.6209 for COM, 0.0000–0.8024 for P1, 0.0000–15.7558 for MP, 0.0111–1.2627 for Onset, 0.0003–1.0508 for P2, and 0.0021–0.5917 for FP.

Statistical analyses were employed to evaluate low-temperature flow properties and DSC parameters with respect to

TABLE 1
Low-Temperature Flow Properties of Methyl Soyate (SME), Methyl Tallowate (TME), SME/TME Admixtures and Winterized SME. DFI-200 and Winterflow Loading = 2000 ppm (before winterization for winterized formulations)[a]

Formulation	CP (°C)	PP (°C)	CFPP (°C)	LTFT (°C)
SME	0[b]	−2[b]	−3[c]	2[c]
SME + DFI-200	−1[b]	−16[b]	−4[d]	−4
SME + Winterflow	−1[b]	−17[b]	−2[d]	−4
Winterized SME (Trial #1)	−20[b]	−21[b]	−17	−16[e]
Winterized SME + DFI-200	−11[b]	n.d.	n.d.	n.d.
Winterized SME + Winterflow	−11[b]	n.d.	n.d.	n.d.
95:5 (vol/vol) SME/TME	2[c]	−4[c]	−1	n.d.
90:10 (vol/vol) SME/TME	1[c]	−1[c]	−3	n.d.
80:20 (vol/vol) SME/TME	2[c]	1[c]	0[c]	3[c]
70:30 (vol/vol) SME/TME	4[c]	1[c]	−1	n.d.
TME	13	15	8	19

[a]CP, cloud point; PP, pour point; CFPP, cold-filter plugging point; LTFT, low-temperature flow test; n.d., not determined.
[b]Data from Reference 9.
[c]Data from Reference 3.
[d]Data from Reference 6.
[e]Measured for mixture of products from winterization Trial #1 and Trial #2.

TABLE 2
Results from Differential Scanning Calorimetry (DSC) Analysis of SME, TME, SME/TME Admixtures; and Winterized SME. DFI-200 and Winterflow Loading = 2000 ppm (before winterization for winterized formulations)[a]

Formulation	COM (°C)	P1 (°C)	MP (°C)	Onset (°C)	P2 (°C)	FP (°C)
SME	6.0	2.7	–11.1	–6.5	–8.0	–6.6
SME + DFI-200	6.4	–0.9	–3.6	–7.1	–7.9	–7.4
SME + Winterflow	5.4	1.4	–7.0	–6.9	–8.1	–7.6
Winterized SME (Trial #1)	9.6	–10.9	–24.6	–19.9	–20.8	–20.0
Winterized SME (Trial #2)	10.7	–11.9	–23.3	–21.1	–22.4	–21.2
Winterized SME + DFI-200	8.9	–0.4	–0.9	–16.6	–17.2	–16.7
Winterized SME + Winterflow	5.9	–5.5	–19.4	–15.1	–15.9	–15.4
95:5 (vol/vol) SME/TME	6.8	3.7	–11.7	–5.1	–7.0	–5.3
90:10 (vol/vol) SME/TME	8.1	4.9	–9.2	–4.4	–6.4	–4.7
80:20 (vol/vol) SME/TME	9.4	6.4	–1.2	–2.1	–4.6	–2.8
70:30 (vol/vol) SME/TME	10.9	7.5	–4.8	–0.1	–2.1	–0.3
TME	17.2	13.9	3.4	7.9	5.9	7.7

[a]COM, completion of melt onset temperature; P1, minimal high melting peak temperature; MP, melting point; Onset, crystallization onset temperature; P2, maximal high freezing peak temperature; FP, freezing point. See Table 1 for other abbreviations.

corresponding formulations (see Tables 1 and 2). Two sample *t*-tests (unequal variances) were conducted to determine whether a given low-temperature flow property might be correlated to a given DSC parameter. Least-squares regression analyses were conducted to infer linear and second-order polynomial fitted equations for calculating low-temperature flow properties from individual DSC parameters.

RESULTS AND DISCUSSION

Low-temperature flow properties. Table 1 is a summary of CP, PP, CFPP, and LTFT data for each of the formulations examined in this work. A majority of these results was reported in earlier studies (3,6,9). However, comparison in this work with new data is justified because identical samples were employed in acquisition of all data.

Measurement of DSC parameters. Figure 1 is a schematic showing how COM, P1, and MP were inferred from the DSC heating scans, while Figure 2 shows how Onset, P2, and FP were inferred from cooling scans. Analysis of scans was conducted with respect to β-form peaks in the high-temperature melting/freezing region (exceeding –40°C). COM was defined as the intersection of a line tangent to the scan at the point of sharpest slope and a line tangent to a segment of baseline on the "hot side" of the melting peak. Onset was the intersection of similar lines on the hot side of the freezing peak. P1 was the point of minimal heat flow (W/g) in the melting peak, while P2 was the point of maximal heat flow in the freezing peak. MP was defined as the point where a line tangent to the scan at the point of sharpest slope on the "cool side" of the melting peak intersects a line across the base of the peak. FP was the point where a tangent on the hot side of the freezing peak intersects a line across the base of that peak. Note that Onset and FP are not necessarily equivalent, due to discrepancies in slope for lines drawn tangent to the baseline and across the base of the peak.

The curve for nonwinterized SME in Figure 1 shows split peaks between –30 and +10°C. This indicates that more than one type of phase transition occurred during the melting tran-

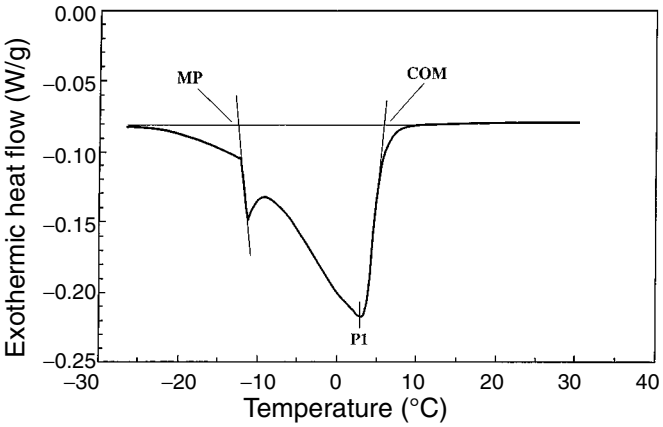

FIG. 1. Differential scanning calorimeter (DSC) heating scan of nonwinterized methyl soyate (SME) at 5°C/min. COM, completion of melt onset temperature, P1, minimal high melting peak temperature; MP, melting point.

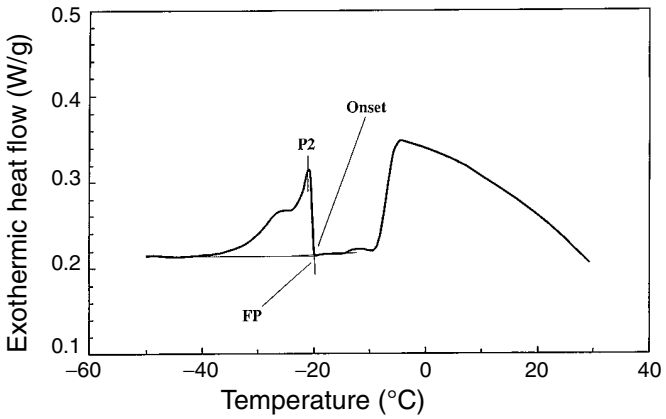

FIG. 2. DSC cooling scan of winterized SME at 5°C/min. Onset, crystallization onset temperature; P2, maximal high freezing peak temperature; FP, freezing point. See Figure 1 for other abbreviations.

sition. This behavior is consistent with mixtures of fatty compounds, such as mixtures of unsaturated and saturated long-chain methyl esters. Each formulation tested showed melting behavior consistent with that shown in Figure 1. Furthermore, the appearance of the split peak caused significant scatter with respect to MP. For example, a 70:30 (vol/vol) SME/TME admixture gave a lower MP = −4.8°C than might be expected given the result for an 80:20 admixture (MP = −1.2°C). Also, interpretation of heating scan parameters for winterized SME formulations was complicated by appearance of two or more separate peaks and occurrence of high-melting peaks at temperatures exceeding those for nonwinterized formulations (discussed below).

The scan in Figure 2 shows that winterized SME underwent at least two distinct phase transitions between −30°C and +10°C. The first transition occurred at temperatures above −10°C and was observed for each formulation listed in Table 2. An earlier study (9) reported that this phenomenon was likely a liquid–liquid transition similar to the formation of liquid crystals. The second transition occurred at temperatures below −10°C and was consistent with a freezing peak. Cooling scans for SME, SME–TME admixtures, and winterized SME were analyzed with respect to the second transition (for example, the peak at P2 = −22°C in Fig. 2).

Comparison of low-temperature flow properties vs. DSC parameters. Table 3 is a summary of results from statistical comparison of CP, PP, CFPP, and LTFT against COM, P1, MP, Onset, P2, and FP by two-sample *t*-tests with unequal variances. Results gave a two-tail probability (*P*) for accepting the hypothesis of a correlation between a given low-temperature flow property and a DSC parameter. If $P > 0.05$, then the corresponding hypothesis could not be rejected.

Data for nonwinterized SME + Winterflow and SME + DFI-200 formulations was omitted from comparison with PP data because cold-flow improvers decreased PP without significantly affecting the location, shape, or size of peaks in the DSC scans. Otherwise, results consistently showed correlation may exist between PP and each DSC parameter except COM ($P = 0.006$). With respect to Onset, the hypothesis was acceptable with very high probability ($P = 0.996$). Although not listed in Table 3, results from paired two-sample *t*-testing of Onset and PP data gave $P = 0.992$. Comparison of FP and PP data also gave very high probabilities ($P = 0.944$ for two-sample testing and 0.872 for paired two-sample testing) favoring correlation.

Comparisons of CP, CFPP, and LTFT were conducted without omitting data from Tables 1 and 2. Data in the CP column of Table 3 showed that the most favorable parameter for correlation was P1 ($P = 0.238$), followed by Onset, FP, MP, and P2 in descending order. The most favorable parameter for correlation with CFPP was Onset ($P = 0.463$), followed by FP, P2, MP, and P1. COM was rejected as a parameter for CP ($P = 0.003$) and CFPP ($P = 0.001$). The most favorable parameter for correlation with LTFT column was P1 ($P = 0.757$), followed by Onset, FP, MP, P2, and COM.

Although MP gave *P* values indicating correlation might exist with each of the low-temperature flow properties, σ^2 values of MP data were relatively large for several formulations (Table 2). Examples of formulations with relatively large σ^2 values included nonwinterized SME + Winterflow ($\sigma^2 = 9.8321$), and 95:5 (vol/vol) SME/TME ($\sigma^2 = 12.1669$) and 70:30 (vol/vol) SME/TME ($\sigma^2 = 15.7558$) admixtures. Deviations between replicates were likely caused by secondary and tertiary phase transitions such as irreversible cooling effects induced by precooling the sample. Upon reheating, the irreversibly altered sample gave split peaks, leading to scatter in MP results as previously discussed. As a result, accurate MP measurement directly from DSC heating curves may be problematic for biodiesel.

These results qualitatively confirmed the utility of DSC heating and cooling scans in evaluation of low-temperature flow properties and behavior of methyl esters. The relative diversity between formulations investigated in this work indicates that DSC analyses may be applied to biodiesel derived from feedstocks that vary significantly in fatty acid composition as well as to untreated and winterized biodiesel.

Calibration of CP. Figure 3 is a plot of results from least-squares regression of CP vs. COM and Onset. In most cases calibration curves deviate from raw data by less than 2°C. Three notable exceptions in the CP vs. COM data at CP < −10°C were omitted from regression analysis.

Table 4 is a summary of results from regression analyses for calibration of CP with respect to each DSC parameter. These results show P2 to be the most accurate predictor for CP (correlation coefficient, $R^2 = 0.980$; standard error of the *y*-estimate, $\sigma_y = 1.28$). Not surprisingly, the least accurate parameter was MP ($R^2 = 0.474$; $\sigma_y = 6.46$).

In general, DSC cooling scan parameters yielded more reliable calibration curves. Although accuracy of these parameters was P2 > FP > Onset, in descending order, Onset may be

TABLE 3
Statistical Comparison of Low-Temperature Flow Properties with Corresponding DSC Parameters: Two-Sample *t*-Tests with Unequal Variances[a]

P	CP	PP	CFPP	LTFT
<0.05	COM	COM	COM	—
0.05–0.20	Onset > FP > MP > P2	P1	MP > P1	COM
0.20–0.50	P1	—	Onset > FP > P2	Onset > FP > MP > P2
>0.50	—	Onset > FP > P2 > MP	—	P1
>0.90	—	FP, Onset	—	—
Best parameter (max *P* value)	P1 ($P = 0.238$)	Onset ($P = 0.996$)	Onset ($P = 0.463$)	P1 ($P = 0.757$)

[a]*P* = two-tail probability from two-sample *t*-tests with unequal variances. See Tables 1 and 2 for other abbreviations.

preferred because it gave linear fit with respect to CP, while P2 and FP each gave second-order polynomial fits. Each of the cooling scan parameters predicted CP values within ASTM guidelines for precision (≤2°C for distillate oils; ≤6°C for other oils) (14).

It has already been noted that Onset data from DSC cooling curves have successfully been employed to determine CP of distillate fuel. An earlier study (11) reported an $R^2 = 0.989$ for linear regression of CP-Onset data for diesel fuel. Although results reported in Table 4 ($R^2 = 0.956$) do not conclusively indicate a linear correlation, they show that CP of biodiesel may be reliably calculated from Onset with σ_y <2°C, a value within ASTM guidelines for precision.

With respect to σ_y, one DSC heating scan parameter, COM, was singularly the most accurate parameter for predicting CP. However, the three data points in Figure 3 omitted from regression analysis each represented winterized SME formulations with and without additives. These points were omitted because they showed an increase in COM with respect to nonwinterized formulations. Given that winterization decreases CP, the observed increase in COM was counterintuitive. An earlier study (9) reported that these effects may be due to formation of solid crystals with an increased concentration of saturated methyl esters in winterized SME. Altering the composition of solid crystals may produce a supersaturation effect that necessitates more time and slightly higher temperatures (more energy) to complete the melting, relative to solid crystals that may contain higher concentrations of occluded unsaturated methyl esters. Thus, this work shows that DSC heating scans may only be reliable for predicting CP of nonwinterized methyl esters.

Results pertaining to prediction of CP from COM and Onset confirm those reported in earlier studies (6,9). The latter reference study reported the following for predicting CP from cooling scans:

$$CP = 1.3653(Onset) + 9.1 \quad [1]$$

with $R^2 = 0.8834$ and $\sigma_y = 1.8$. Equation 1 was derived from analysis of primarily winterized SME fractions, while the analogous equation derived in this work (Table 4) was based on results from nonwinterized SME and SME-additive mixtures, winterized SME and SME-additive mixtures, and nonwinterized SME–TME admixtures. Statistical comparison of regressions lines between the equation derived in this work and Equation 1 indicated that the lines may be coincidental. Thus, CP of nonwinterized and winterized biodiesel may be linearly calibrated to and accurately predicted from Onset measurements.

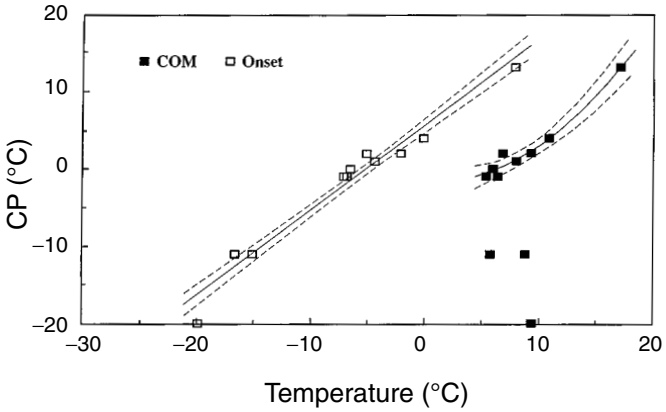

FIG. 3. Calibration of cloud point (CP) with respect to COM (■) and Onset (□). Solid lines (—) = calibration curve; dashed lines (- - -) = confidence intervals (±0.025). See Figures 1 and 2 for other abbreviations.

Overall, these results consistently show that DSC cooling scan parameters were accurate and more reliable than heating scan parameters for predicting CP of nonwinterized and winterized methyl esters studied in this work. Thus, DSC cooling scan parameters should be employed to predict CP of biodiesel.

Calibration of PP, CFPP, and LTFT. Table 5 is a summary of results from least-squares regression analyses of PP, CFPP, and LTFT vs. each DSC parameter. Similar to *t*-testing of data pairs, nonwinterized SME + DFI-200 and SME + Winterflow formulations were omitted from PP-curve analyses because the cold-flow improvers decreased PP without greatly altering the melting/freezing peaks. Similar to analysis of CP-COM curves, the three winterized SME formulations were omitted from regression of CFPP and LTFT vs. COM curves.

Results from PP, CFPP, and LTFT regression analyses were comparable to those for CP with respect to comparing heating against cooling scan parameters. Calibrations with cooling scan parameters gave $R^2 = 0.924$–0.973 and $\sigma_y = 1.67$–3.15. In particular, regressions with respect to Onset

TABLE 4
Regression Analysis of CP Calibration Curves {$CP = a_0 + a_1(x) + a_2(x^2)$}[a]

x	Order	*df*	a_0	a_1	a_2	R^2	σ_y
COM[b]	2	5	–2.0215	–0.0136	0.0515	0.958	0.94
Onset	1	9	5.5997	1.1014	—	0.956	1.87
P1	1	9	–4.6793	1.2842	—	0.899	2.83
P2	2	8	7.5654	0.8947	–0.0172	0.980	1.28
MP	1	9	4.3738	0.7798	—	0.474	6.46
FP	2	8	6.0756	0.8836	–0.0160	0.972	1.50

[a]*df*, degrees of freedom; a_i, *i*th regression coefficient; R^2, correlation coefficient; $\sigma_{y'}$ standard error of the *y*-estimate. See Tables 1 and 2 for other abbreviations.
[b]For nonwinterized esters only.

TABLE 5
Regression Analyses of PP, CFPP, and LTFT Calibration Curves {$y = a_0 + a_1(x) + a_2(x^2)$}[a]

y	*x*	Order	*df*	a_0	a_1	a_2	R^2	σ_y
PP[b]	COM	1	5	–17.7433	1.6657	—	0.208	9.42
	Onset	1	5	3.8151	1.2489	—	0.970	1.83
	P1	1	5	–7.1688	1.3850	—	0.960	2.11
	P2	1	5	6.4769	1.3071	—	0.973	1.74
	MP	1	5	7.9463	1.1271	—	0.900	3.34
	FP	1	5	4.2119	1.3897	—	0.963	2.04
CFPP	COM[c]	2	5	–0.5750	–0.7671	0.0741	0.871	1.38
	Onset	1	7	1.7914	0.8629	—	0.933	1.69
	P1	1	7	–5.4252	0.9328	—	0.918	1.87
	P2	1	7	3.5171	0.9085	—	0.934	1.67
	MP	1	7	3.3153	0.7443	—	0.797	2.94
	FP	1	7	2.0487	0.8624	—	0.923	1.81
LTFT	COM[c]	2	2	–7.2799	0.5533	0.0567	0.865	3.46
	Onset	1	4	7.2657	1.2071	—	0.941	2.78
	P1	1	4	–2.5078	1.3322	—	0.941	2.77
	P2	1	4	9.3338	1.2213	—	0.924	3.15
	MP	1	4	7.7487	1.1177	—	0.655	6.71
	FP	1	4	7.7733	1.2227	—	0.954	2.44

[a]See Tables 1, 2, and 4 for abbreviations.
[b]Omitting nonwinterized mixtures of esters and PP depressants.
[c]For nonwinterized esters only.

were comparable to results reported for diesel fuels (11). Calibrations with heating scan parameters gave $R^2 = 0.208–0.941$ and $\sigma_y = 1.37–9.42$. Although more accurate results with respect to σ_y values were obtained from heating scan parameters, cooling scan parameters were more reliable with respect to R^2 values.

Differences in order of polynomial fits precluded comparison of CFPP or LTFT calibration curves with respect to COM and Onset parameters. Comparison of PP calibration curves showed that COM and Onset had the largest deviation from each other. This may be exemplified by noting that constant a_0 predicted by regression was <0 for COM and >0 for Onset. The scan rate (5°C/min) typically caused a lagging effect between the actual melting or freezing transition and appearance of a peak in the scan. Studies with triglycerides have reported that variances in Onset were likely caused by dependence of nucleation on scan rate (18). Statistical testing of the hypothesis that PP calibration curves for COM and Onset may be parallel was precluded by dissimilar variances of the residuals (σ_y^2).

Comparison of regression lines with respect to P1 and P2 parameters indicated that these curves may be parallel. PP ($P = 0.610$), CFPP ($P = 0.855$), and LTFT ($P = 0.626$) calibration curves each favored the hypothesis of equivalent slopes. However, each comparison rejected the hypothesis of coincidental curves due to lagging effects induced by scan rate on measuring P1 and P2.

Comparison of regression curves for MP and FP parameters showed that the hypothesis of parallel curves could not be rejected for PP ($P = 0.194$) and CFPP ($P = 0.472$) calibration curves. Comparison of CFPP curves also favored the hypothesis of coincidental lines for MP and FP ($P \sim 0.10$). Although slopes and intercepts for LTFT curves were comparable, statistical comparison was precluded by dissimilar σ_y^2 values. In contrast to earlier comparison of heating and cooling scan parameters, lagging effects induced by scan rate on the MP- and FP-based curves were apparently less significant.

These results show that PP may be most accurately predicted by calibration with P2 followed closely by Onset; that CFPP may be most accurately predicted by calibration with either P2 or Onset followed closely by FP; and that LTFT may be most accurately predicted by calibration with FP followed closely by P1 or Onset. These conclusions were drawn by maximizing R^2 and minimizing σ_y values. Remembering that regression of PP curves omitted nonwinterized SME + cold-flow improver formulations, cooling scan parameters gave the most accurate and reliable correlations for predicting low-temperature flow properties of methyl esters studied in this work. Therefore, DSC cooling scan parameters should be employed to predict PP, CFPP, and LTFT of biodiesel.

Comparison of CP and LTFT calibrations. It was noted in the introduction that an empirical 1:1 correlation exists between LTFT and CP for SME and SME/distillate blends. Statistical comparison of CP and LTFT Onset calibration curves (Table 4) agreed with this correlation by accepting the hypothesis of coincidental lines ($P = 0.505$ for equivalent slopes; 0.263 for equivalent intercepts). As a result, the following equation was derived:

$$CP = LTFT = 1.1441(Onset) + 6.2 \quad [2]$$

The slope = 1.1441 was an average value using a weight factor based on the sum of squares of deviations of Onset data from their mean value. The intercept = 6.2 was an average

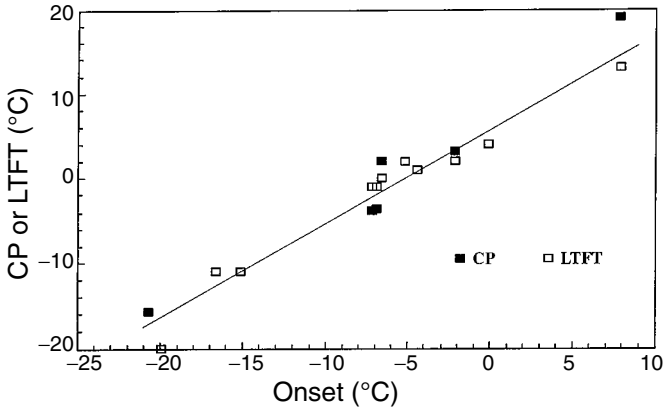

FIG. 4. Comparison of low-temperature flow test (LTFT) and CP data with CP predicted from Onset. Solid line (—) = calibration curve {CP = 1.1014(Onset) + 5.6}. See Figures 2 and 3 for other abbreviations.

value using a weight factor based on the number of data pairs in the combined data sets.

A second comparison between CP and LTFT vs. Onset data and the CP calibration curve [CP = 1.1014(Onset) + 5.6] is shown graphically in Figure 4. These results demonstrate that the CP calibration curve may be employed to predict LTFT. Comparison between LTFT data and those predicted by the CP calibration curve gave a standard deviation (σ) = 2.7°C, a value well within ASTM method D4539 guidelines with respect to precision (maximal reproducibility = 4°C between two independent LTFT measurements) (16).

Comparison of calibration curves with respect to P2 and FP was not possible due to differences in the polynomial orders for CP (second order) and LTFT (first order) calibration curves. Thus, equations analogous to Equation 2 were not derived. Nevertheless, comparison of measured and predicted LTFT data similar to that shown in Figure 4 could be conducted. Estimation of LTFT from the CP calibration curves gave σ = 4.1°C for P2 and σ = 3.6°C for FP.

ACKNOWLEDGMENTS

The author thanks A.L. Callison, D.W. Ehmke, H. Khoury, and R. Zick for their technical assistance in completion of this work.

REFERENCES

1. Chandler, J.E., F.G. Horneck, and G.I. Brown, The Effect of Cold Flow Additives on Low-Temperature Operability of Diesel Fuels, in *SAE Technical Paper Series Paper No. 922186*, Society of Automotive Engineers, Warrendale, PA, 1992.
2. Lewtas, K., R.D. Tack, D.H.M. Beiny, and J.W. Mullin, Wax Crystallization in Diesel Fuel: Habit Modification and the Growth of *n*-Alkane Crystals, in *Advances in Industrial Crystallization*, edited by J. Garside, R.J. Davey, and A.G. Jones, Butterworth-Heineman, Oxford, 1991, pp. 166–179.
3. Dunn, R.O., and M.O. Bagby, Low-Temperature Properties of Triglyceride-Based Diesel Fuels: Transesterified Methyl Esters and Petroleum Middle Distillate/Ester Blends, *J. Am. Oil Chem. Soc. 72*:895–904 (1995).
4. Owen, K., and T. Coley, Diesel Fuel Low-Temperature Characteristics, in *Automotive Fuels Handbook*, Society of Automotive Engineers, Warrendale, PA, 1990, pp. 353–403.
5. McMillan, M.L., and E.G. Barry, Fuel and Vehicle Effects on Low-Temperature Operation of Diesel Vehicles—The 1981 CRC Field Test, in *SAE Technical Paper Series Paper No. 830594*, Society of Automotive Engineers, Warrendale, PA, 1983.
6. Dunn, R.O., and M.O. Bagby, Low-Temperature Filterability Properties of Alternative Diesel Fuels from Vegetable Oils, *Proceedings of the Third Liquid Fuels Conference: Liquid Fuels and Industrial Products from Renewable Resources*, edited by J.S. Cundiff, E.E. Garett, C. Hansen, C. Peterson, M.A. Sanderson, H. Shapouri, and D.L. Van Dyne, American Society of Agricultural Engineers, St. Joseph, MI, 1996, pp. 95–103.
7. Dunn, R.O., M.W. Shockley, and M.O. Bagby, Improving the Low-Temperature Properties of Alternative Diesel Fuels: Vegetable Oil-Derived Methyl Esters, *J. Am. Oil Chem. Soc. 73*:1719–1728 (1996).
8. Lee, I., L.A. Johnson, and E.G. Hammond, Reducing the Crystallization Temperature of Biodiesel by Winterizing Methyl Soyate, *Ibid. 73*:631–636 (1996).
9. Dunn, R.O., M.W. Shockley, and M.O. Bagby, Winterized Methyl Esters from Soybean Oil: An Alternative Diesel Fuel with Improved Low-Temperature Flow Properties, in *SAE Special Publication SP-1274: State of Alternative Fuel Technologies—1997, Paper No. 971682*, Society of Automotive Engineers, Warrendale, PA, 1997, pp. 133–142.
10. Heino, E.-L., Determination of Cloud Point for Petroleum Middle Distillates by Differential Scanning Calorimetry, *Thermochim. Acta 114*:125–130 (1987).
11. Claudy, P., J.-M. Létoffé, B. Neff, and B. Damin, Diesel Fuels: Determination of Onset Crystallization Temperature, Pour Point and Filter Plugging Point by Differential Scanning Calorimetry. Correlation with Standard Test Methods, *Fuel 65*:861–864 (1986).
12. Noel, F., Thermal Analysis of Lubricating Oils, *Thermochim. Acta 4*:377–392 (1972).
13. Redelius, P., The Use of DSC in Predicting Low Temperature Behaviour of Mineral Oil Products, *Ibid. 85*:327–330 (1985).
14. ASTM D2500: Standard Test Method for Cloud Point of Petroleum Oils, in *Annual Book of ASTM Standards*, Vol. 05.02, American Society for Testing and Materials, Philadelphia, PA, 1991, pp. 268–270.
15. ASTM D97: Standard Test Method for Pour Point of Petroleum Oils, in *Ibid.*, Vol. 05.01, American Society for Testing and Materials, Philadelphia, PA, 1993, pp. 85–88.
16. ASTM D4539: Standard Test Method for Filterability of Diesel Fuels by Low-Temperature Flow Test (LTFT), in *Ibid.*, Vol. 05.03, American Society for Testing and Materials, Philadelphia, PA, 1991, pp. 446–450.
17. IP 309: Cold Filter Plugging Point of Distillate Fuels, in *IP Standard Methods for Analysis and Testing of Petroleum and Related Products*, The Institute of Petroleum, London, 1991.
18. Cebula, D.J., and K.W. Smith, Differential Scanning Calorimetry of Confectionery Fats. Pure Triglycerides: Effects of Cooling Rate and Heating Rate Variation, *J. Am. Oil Chem. Soc. 68*:591–595 (1991).

[Received June 23, 1998; accepted September 29, 1998]